

A CHANDRA VIEW OF THE NORMAL S0 GALAXY NGC 1332: I. AN UNBROKEN, STEEP POWER LAW LUMINOSITY FUNCTION FOR THE LMXB POPULATION.

PHILIP J. HUMPHREY AND DAVID A. BUOTE

Department of Physics and Astronomy, University of California at Irvine, 4129 Frederick Reines Hall, Irvine, CA 92697-4575

Draft version October 29, 2018

ABSTRACT

Chandra *ACIS-S3* observations of the nearby S0 galaxy NGC 1332 resolve much of the X-ray emission into 73 point-sources, of which 37 lie within the D_{25} isophote. The remaining galaxy emission comprises hot, diffuse gas and unresolved sources and is discussed in two companion papers. The point-source luminosity function (XLF) shows the characteristic break seen in other early-type galaxies at $\sim 2 \times 10^{38}$ erg s⁻¹. After applying corrections for detection incompleteness at low luminosities due to source confusion and contamination from diffuse galactic emission, the break vanishes and the data are well-described as a single power law. This result casts further doubt on there being a “universal” XLF break in early-type galaxies marking the division between neutron-star and black-hole systems. The logarithmic slope of the differential XLF (dN/dL), $\beta = 2.7 \pm 0.5$, is marginally ($\sim 2.5\sigma$) steeper than has been found for analogous completeness-corrected fits of other early-type galaxies but closely matches the behaviour seen at high luminosities in these systems. Two of the sources within D_{25} are Ultra-luminous X-ray sources (ULX), although neither have $L_X > 2 \times 10^{39}$ erg s⁻¹. The absence of very luminous ULX in early-type galaxies suggests a break in the XLF slope at $\sim 1-2 \times 10^{39}$ erg s⁻¹, although the data were not of sufficient quality to constrain such a feature in NGC 1332. The sources have a spatial distribution consistent with the optical light and display a range of characteristics that are consistent with an LMXB population. The general spectral characteristics of the individual sources, as well as the composite source spectra, are in good agreement with observations of other early-type galaxies, although a small number of highly-absorbed sources are seen. Two sources have very soft spectra, two show strong variability, indicating compact binary nature and one source shows evidence of an extended radial profile. We do not detect a central source in NGC 1332, but we find a faint ($L_X = 2 \pm 1 \times 10^{38}$ erg s⁻¹) point-source coincident with the centre of the companion dwarf galaxy NGC 1331.

Subject headings: galaxies: elliptical and lenticular, cD — galaxies: individual (NGC 1332) — X-rays: binaries — X-rays: galaxies

1. INTRODUCTION

Prior to the launch of *Chandra* only a small number of the very brightest point-sources in early type galaxies could be resolved from the diffuse galactic emission (Fabbiano 1989; Colbert & Mushotzky 1999; Roberts & Warwick 2000). The study of their point-source populations was therefore restricted to the average, composite properties inferred by decomposing the emission into a number of spectral or spatial model components (e.g. Matsushita et al. 1994; Brown & Bregman 2001). The advent of *Chandra* has revolutionized this field, however, allowing a large fraction of the sources to be resolved and studied directly (for a recent review, see Fabbiano & White 2003). Extragalactic point-sources most probably represent an heterogeneous mixture of different source types, although the old stellar populations characteristic of early-type galaxies suggest a predominantly low-mass X-ray binary (LMXB) nature. As endpoints of stellar evolution, the properties of X-ray binaries are a crucial diagnostic for the evolution of the stars as a whole within the galaxy. Although the data are generally of insufficient quality to investigate fully for each source the rich, diagnostic phenomenology of Galactic LMXB (White et al. 1995), in some cases it has been possible to identify variability (e.g. Sarazin et al. 2001; Kraft et al. 2001) and the spectral signatures of black-hole binaries (e.g. Makishima et al.

2000; Humphrey et al. 2003).

In order to study the properties of the X-ray point-source population as a whole, it is common practice to consider the X-ray luminosity function (XLF) (e.g. Sarazin et al. 2001; Blanton et al. 2001; Zezas & Fabbiano 2002), the shape of which is a strong function of the age of the stellar population (Kilgard et al. 2002; Belczynski et al. 2003). Between early-type galaxies, there is remarkable similarity in the shape of the XLF (Kim & Fabbiano 2003b), which is typically found to be a steep power law with a break occurring around $2-4 \times 10^{38}$ erg s⁻¹ and a high-luminosity slope, $\beta \simeq 2-3$ (Sarazin et al. 2001; Blanton et al. 2001; Kraft et al. 2001; Colbert et al. 2003). These slopes are also broadly consistent with old stellar populations in M31 (Kong et al. 2003). It has been suggested that the presence of breaks at luminosities at around the Eddington limit of a $1.4M_{\odot}$ neutron star ($L_{\text{EDD}} = 2-4 \times 10^{38}$ erg s⁻¹, depending on the composition of the accreting matter and the neutron-star equation of state: Paczyński 1983) may arise from a division between neutron-star and black-hole systems (e.g. Sarazin et al. 2001). However in the elliptical galaxy NGC 720, a substantially higher luminosity break, at $\sim 1 \times 10^{39}$ erg s⁻¹ was found instead by Jeltama et al. (2003). Kim & Fabbiano (2003a) pointed out that in the elliptical galaxy NGC 1316, a break is arises only if no correction is made for point-

source detection incompleteness. Applying this correction to a sample of early-type galaxies, Kim & Fabbiano (2003b) found a similar result, although they still found marginal evidence of a break at $\sim 5 \times 10^{38}$ erg s $^{-1}$. This luminosity is sufficiently high, however, to cast further doubt upon the idea that it marks the division between neutron-star and black-hole binaries.

At the extreme end of the XLF are the so-called ‘‘Ultra Luminous X-ray sources’’ (ULX), which are non-nuclear objects with luminosities exceeding 10^{39} erg s $^{-1}$, sometimes reaching as high as 10^{41} erg s $^{-1}$ (e.g. Fabbiano 1989; Makishima et al. 2000; Zezas et al. 2002; Davis & Mushotzky 2003). They have been found in galaxies of all morphological types (Colbert & Ptak 2002), although there is a strong association between ULX and star-formation so that their specific frequency is far lower in early-type galaxies (Kilgard et al. 2002; Humphrey et al. 2003; Irwin et al. 2003b). However, in the otherwise normal elliptical NGC 720, Jeltama et al. (2003) found a remarkable population of 9 ULXes. The nature of ULX is somewhat enigmatic. Although the less extreme objects ($L_X \sim 1\text{--}2 \times 10^{39}$ erg s $^{-1}$) are consistent with isotropic emission from Eddington-limited black-hole binaries with compact-object masses $\sim 10\text{--}20M_\odot$, there has been much debate over whether the most luminous objects represent ‘‘Intermediate mass black holes’’ with masses $\gtrsim 100M_\odot$, super-Eddington emission from sources in the thermal-timescale mass-transfer phase, or beamed emission from lower-luminosity sources (Colbert & Mushotzky 1999; King et al. 2001; King 2002).

Another feature of the LMXB population of particular interest is its possible association with globular clusters (GCs), since it provides valuable insight into X-ray binary formation. The fraction of the extragalactic LMXB identified with GCs varies considerably between galaxies, from $\sim 20\text{--}70\%$ (Angelini et al. 2001; Kundu et al. 2002; Sarazin et al. 2001). Nonetheless, there is evidence that the frequency of at least part of the LMXB population correlates with the numbers of GCs so that $\sim 4\%$ of all GCs contain an LMXB, consistent with the Milky Way (Kundu et al. 2003; Sarazin et al. 2003). These authors also found evidence that LMXB favour brighter, redder GCs.

In this paper, we analyse with *Chandra* the hitherto unresolved point-source population of the lenticular galaxy NGC 1332. Using *Rosat PSPC* data of this galaxy, Buote & Canizares (1996, hereafter BC) found elongation of the X-ray isophotes and demonstrated that the galaxy mass profile was marginally inconsistent with the optical light, indicating the presence of a substantial dark matter halo. Unfortunately, most of the point-source population could not be resolved, so that it was necessary to estimate limits for the unresolved point-source contribution to the X-ray emission, and tight constraints on the shape of the dark matter halo could not be obtained. Using *ASCA* data Buote & Canizares (1997) found a hard spectral component in the integrated stellar emission, indicating a significant contribution from unresolved LMXB, although this did not allow these sources to be studied in detail. *Chandra* allows us for the first time to separate a large fraction of the LMXB from the diffuse emission of NGC 1332, and to study them directly. The properties of the diffuse gas and the mass distribu-

tion are discussed separately in two companion papers (Humphrey et al. 2004; Buote et al. 2004, hereafter Papers I and II, respectively).

In order to determine the properties of the stellar population accurately, it is important to adopt a reliable distance estimate (c.f. NGC 4038/9, for which a recently revised distance estimate would reduce the reported ULX population threefold; Saviane et al. 2003). For NGC 1332, distances determined both by surface brightness fluctuations (SBF) and the globular cluster luminosity function (GCLF) are in excellent agreement, being 23 ± 3 Mpc and 22 ± 6 Mpc, respectively (Tonry et al. 2001; Kundu & Whitmore 2001). All errors quoted here, and subsequently, are 90% confidence limits unless otherwise stated.

2. OBSERVATIONS AND DATA ANALYSIS

The region of sky containing NGC 1332 was observed with the ACIS instrument aboard *Chandra* between 2002 September 19 10:39 and September 20 02:59 UTC, the galaxy being centred on the S3 chip, for a nominal ~ 60 ks exposure. An additional observation made between September 18 02:56 and 08:27 UTC, for a nominal 20 ks exposure, was heavily contaminated by flaring of the background and so we present results only for the better-quality dataset. For data-reduction, we used the *CIAO* 3.0.1 and *Heasoft* 5.2 suites of software tools, and for spectral analysis we used *XSPEC* 11.2.0 and *ISIS* 1.1.5. In order to use the most up-to-date calibration, we reprocessed the Level-1 data, following the standard *Chandra* threads¹. We corrected a time-dependent drift in the gain with the `apply_gain`² task. To identify periods of unusually high background for which the degradation in signal-to-noise can affect analysis, a lightcurve was generated from source-free regions of the active chips and examined by eye for ‘‘flares’’. For much of the observation there was evidence of low-level flaring ($\Delta R/R \sim 20\%$, where R is the count-rate). For point-source identification and characterisation, we found the S/N improvement from reducing the background level (by $\sim 10\%$) was outweighed by the reduction in the exposure-time (by $\sim 30\%$) if we excised data during the strongest flares. We therefore used the entire observation, giving a total exposure time of 57 ks. We have systematically confirmed that including the flaring did not bias our results. A more thorough discussion of the flaring is given in Paper II. Fig. 1 shows the image of the inner part of the S3 chip, which has been flat-fielded with an exposure-map generated with *CIAO* at 1.0 keV (approximately the peak energy of the diffuse emission), and smoothed with the *CIAO* task `csmooth` (taking the default parameter values). A number of bright point-sources are clearly visible in the X-ray data. For comparison purposes the Digitized Sky Survey (DSS) optical image is also shown.

3. POINT SOURCE DETECTION

Point-source detection was performed using the *CIAO* tool `wavdetect` (Freeman et al. 2002). In order to improve the likelihood of identifying sources with peculiarly hard or soft spectra, full-resolution images were created

¹ <http://cxc.harvard.edu/ciao/threads/index.html>

² http://cxc.harvard.edu/cont-soft/software/corr_tgain.1.0.html

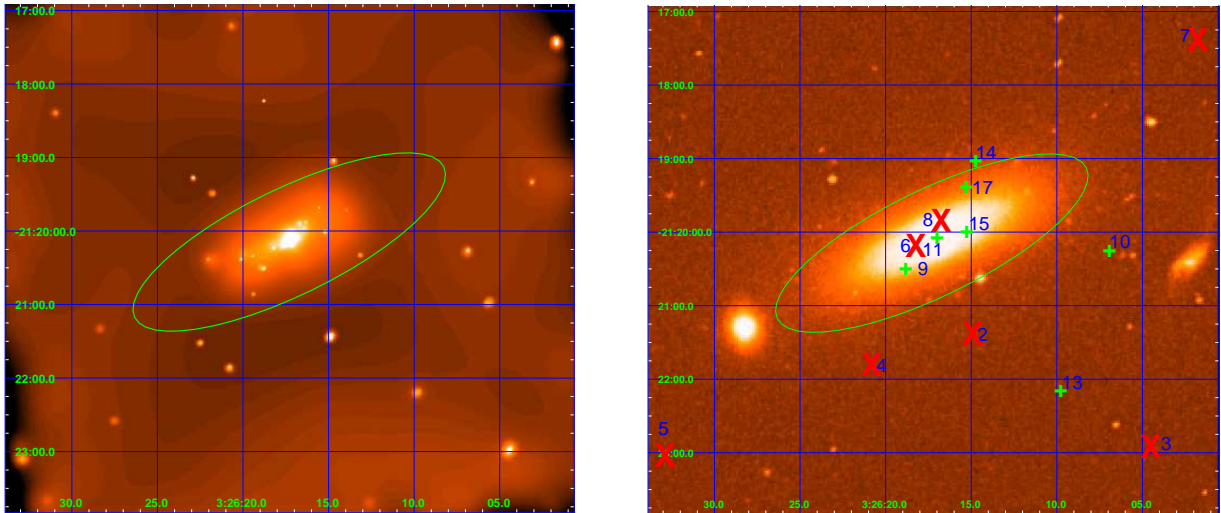


FIG. 1.— left panel: False colour, smoothed image of the central part of the S3 chip. The image was initially flat-fielded with an exposure-map created at 1 keV (peak energy). Overlaid is the D₂₅ ellipse taken from de Vaucouleurs et al. (1991), but the position angle has been altered to 116° to agree with BC. Right panel: the DSS optical image, overlaid with the D₂₅ ellipse and, following Humphrey et al. (2003), the positions of X-ray sources with $L_X > 10^{39}$ erg s⁻¹ (X) and those with $5 \times 10^{38} < L_X < 10^{39}$ erg s⁻¹ (+). The identification numbers of a selection of interesting sources are given on the figure. The bright galaxy to the left of NGC 1332 is NGC 1331.

of the region of the *ACIS* focal-plane containing the S3 chip in three different energy-bands (0.1–10.0 keV, 0.1–3.0 keV and 3.0–10.0 keV). Sources were detected separately in each image. In order to minimize spurious detections at node or chip boundaries we supplied the detection algorithm with exposure-maps generated at energies 1.7 keV, 1.0 keV and 7 keV respectively (although the precise energies chosen made little difference to the results). The detection algorithm searched for structure over pixel-scales of 1, 2, 4, 8 and 16 pixels, and the detection threshold was set to $\sim 10^{-7}$ spurious sources per pixel (corresponding to ~ 0.1 spurious detections per image). The source-lists obtained within each energy-band were combined and duplicated sources removed, and the final list was checked by visual inspection of the images.

A total of 76 sources were detected on the S3 chip, of which the brightest and most extended was centred within 1'' of the galaxy centroid as given in *NED* (which is accurate to $\sim 2''$). Examination of the azimuthally-averaged radial brightness profile of this “source” (Sect. 4.5) clearly indicated it to be very extended and so we identified this with the central part of the diffuse galactic emission (which had been spuriously identified by *wavdetect* as a point-source due to its being very centrally-peaked). We found that one point-source lay within the B-band 25th magnitude (D₂₅) isophote of NGC 1331 (as listed in de Vaucouleurs et al. 1991). In fact, this source was within 1'' of the galaxy centroid listed in *NED*, but was rather faint (with a count-rate $\sim 4 \times 10^{-4}$ count s⁻¹, corresponding to $L_X \simeq 2 \pm 1 \times 10^{38}$ erg s⁻¹). In addition, one source had no photons in the 0.5–7.0 keV band, suggesting that it was spurious and we therefore omitted it from our list. This left 73 sources on the S3 chip, of which 37 lay within the D₂₅ isophote of NGC 1332 as given in de Vaucouleurs et al. (1991), which has semi-major and semi-minor axes of 2.3' and 0.7', respectively. We adjusted the position angle given in de Vaucouleurs et al. (1991) to 116° to agree with BC and match better the

optical data. The source positions are given in Table 1.

It is interesting to compare our detections with those made with *Rosat*. Using the PSPC, 5 point sources were resolved within the central ring (BC). There are bright *Chandra* detections (which we labelled sources 1, 2 and 6 in Table 1) within 15'' (\sim the PSPC point-spread) of three of these sources. One of the *Rosat* sources would not fit on the S3 chip and the remaining source was close to only one *Chandra* detection, source 71, which was too faint ($L_X \sim 10^{38}$ erg s⁻¹) to have been seen with *Rosat*. This indicates that the source seen with *Rosat* (which may, or may not, correspond with this *Chandra* detection) exhibited dramatic variability over the ~ 6 -year period between the observations.

For each source, lightcurves, spectra and spectral responses were generated using standard *CIAO* tasks. Local background regions were chosen for each source to ensure that contamination from the diffuse galaxy emission (or from the mild flaring) did not bias our results. These were accumulated from annuli centred on the source which were truncated so as to be contained entirely within the same *ACIS* node. They were chosen to cover an area at least 8 times the extraction region, and containing at least 50 photons. We excluded from our background computation photons within a region around each source obtained by scaling the axes of the appropriate 1- σ encircled-energy ellipse by a factor 6 (we excluded such a large region since a few percent of a source’s photons will leak from a region even as large as the 3- σ encircled-energy ellipse, which is problematic in the vicinity of bright sources). To compensate for the progressive quantum-efficiency degradation at low energies due to contamination on the optical blocking filter, we used the `apply_acisabs`³ script to correct the ancillary response files. In order to investigate the possible extent of these sources, dedicated software was used to generate radial brightness profiles centred upon each

³ see http://cxc.harvard.edu/ciao/threads/apply_acisabs

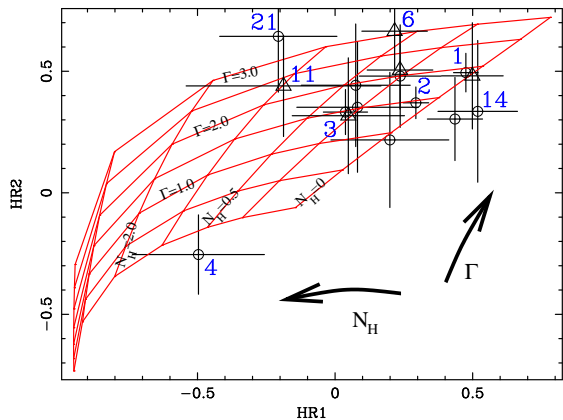


FIG. 2.— Hardness ratios for all sources on the S3 chip with more than 40 counts. Overlaid is a grid of the loci of a simple absorbed power law model as Γ and N_{H} vary. Γ increases upwards, with grid lines shown for $\Gamma=0.0$ – 3.0 in steps of 0.5 . Several representative lines are labelled. N_{H} increases to the left and grid-lines are shown for $N_{\text{H}}=0.0, 0.25, 0.5, 1.0, 2.0, 4.0$ and $8.0 \times 10^{22} \text{cm}^{-2}$, where N_{H} is column in excess of the appropriate Galactic value. Several lines of constant N_{H} are labelled on the figure in units of 10^{22}cm^{-2} . The identification numbers of a selection of interesting sources are indicated on the figure. Sources inside the D_{25} region are shown as triangles, and those outside it are shown as circles.

source and excluding photons from the vicinity of the other detected point-sources. The profiles were extracted initially in very fine, equally-spaced bins ($\sim 0.5''$ width), out to radii as large as $1'$ in order that a reliable background could be estimated. For those sources close to the centre of the galaxy we adopted smaller radii (down to $\sim 0.5'$) to minimize contamination from the diffuse gas, or subsequently included a model to account for the diffuse component when fitting the profile (Sect 4.5).

4. POINT SOURCE PROPERTIES

4.1. Hardness ratios

In order to compare the spectral phenomenology of individual low-count sources it is convenient to construct hardness ratios (e.g. White & Marshall 1984; Kim et al. 1992; Zezas et al. 2002). Background-subtracted counts were measured for each source in three energy-bands, a soft-band (S) from 0.3–1.5 keV, a medium-band (M) from 1.5–3.0 keV and a hard-band (H) from 3.0–5.0 keV, and the hardness ratios HR1 and HR2 were computed. These are defined, respectively, as $\text{HR1} = (S - M)/(S + M)$ and $\text{HR2} = (M - H)/(M + H)$. With these definitions, HR1 is principally sensitive to the hydrogen column-density in the line-of-sight, and HR2 depends upon the steepness of the spectrum, allowing us to construct a useful “colour-colour” diagram (i.e. HR2 *versus* HR1) for NGC 1332 (Fig 2). In order to show how the hardness ratios depend upon the underlying spectrum, we have overlaid a grid showing the loci of simple absorbed power law spectra with a variety of different value of N_{H} and Γ . The position of a given source relative to the grid has implications for its nature; most neutron-star or low-state black hole binaries, for example, would be expected to lie between the $\Gamma = 1$ and the $\Gamma = 2$ lines, whereas high state black holes may be expected to lie above the $\Gamma = 2.5$ line (Humphrey et al. 2003).

In NGC 1332, most of the sources are found to occupy regions consistent with $N_{\text{H}} \simeq$ Galactic

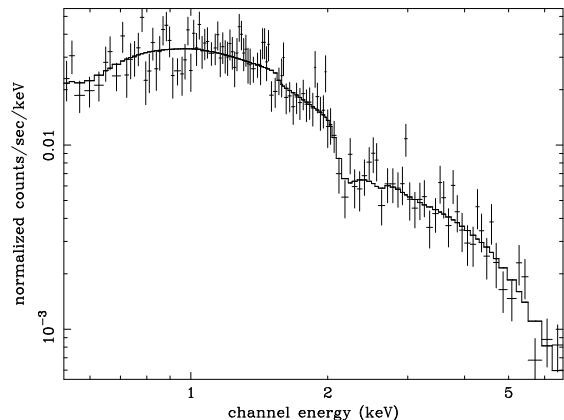


FIG. 3.— Composite spectrum for all sources in the D_{25} region, folded through the instrumental response, and shown with the best-fit bremsstrahlung model.

(Dickey & Lockman 1990) and $\Gamma \simeq 1$ – 2 , as seen in other early-type galaxies. There is considerable scatter, but this merely reflects the few photons detected in each source. Several sources show some evidence of intrinsic, or local, absorption in excess of the Galactic column but there are only two clear outliers (Sources 4 and 21). These are confirmed by spectral-fitting; e.g. Source 4 has $N_{\text{H}} \simeq 10^{22} \text{cm}^{-2}$, in agreement with its hardness-plane position. Sources 6 and 21 have rather soft spectra, although both sources are somewhat harder than the “Supersoft” and “Quasisoft” sources seen in other galaxies (DiStefano & Kong 2003). Based on their colour-colour plane loci, they may be consistent with high-state black hole systems, although this is only one possibility, which will need independent confirmation. Individual spectral-fitting of these sources does not allow the spectra to be constrained very well, but if free, the Γ of a power law fit to each source spectrum does, indeed, rise to $\gtrsim 3.0$, consistent with this picture.

4.2. Composite spectra

In order to examine the overall properties of the source population, and specifically to allow us to separate the unresolved source component from the hot gas during spectral analysis of the diffuse emission (Paper II), we accumulated a composite background-subtracted spectrum of all the point-sources. Response matrices were generated for the data using the *mkwarf* and *mkrmf CIAO* tasks, and corrected for the effects of quantum efficiency degradation at low energies analogously to the individual source spectra. Since all of the brightest sources detected in NGC 1332 were outside the D_{25} region, we separately constructed a composite spectrum for only those sources within this region (thereby preventing our results from being unduly biased by the brightest objects). We rebinned the data to ensure that in each bin there were at least 20 photons (to allow the use of the χ^2 statistic) and a signal-to-noise ratio exceeding 3. Both spectra could be fitted excellently with simple one-component bremsstrahlung or power law models, with N_{H} fixed at the nominal Galactic value, as shown in Table 2. Only for the power law fit to all the S3 sources did freeing the N_{H} led to a modest improvement in the fit statistic. The spectra of the sources within the D_{25} region and those on

the entire chip were only slightly different. For our fit of sources within the D_{25} region, our results were in excellent agreement with those of Irwin et al. (2003a), consistent with the apparently “universal” nature of the composite spectra of the lower-luminosity sources in early-type galaxies.

4.3. Fluxing

To measure the fluxes of the sources, we adopted two complementary techniques (which are effectively equivalent for the lower-counts sources). We rebinned the spectrum of each source to ensure at least 20 photons in each spectral bin (thereby allowing the use of χ^2). When this gave fewer than 4 spectral bins, we instead regrouped the spectrum into ~ 12 bins of approximately equal width in energy and adopted the Cash (maximum likelihood) fit statistic (determining the goodness-of-fit from Monte-Carlo simulations). Initially we fitted a simple power law model, the slope of which matched the co-added source spectra within the D_{25} region. When the “null hypothesis probability” (i.e. the probability of the model fitting the data) was only acceptable at the 5% level or less, we rejected the model and allowed, separately, the photon index and the N_H to be free. In all cases we were then able to obtain statistically acceptable fits. Although more complex spectral models are generally more appropriate for Galactic LMXB (Church & Bałucińska-Church 2001), a simple power law can be used to provide an accurate flux estimate in a relatively narrow energy-band and, for so few photons, more complicated models could not be constrained. To determine the flux errors, we modified the existing *XSPEC*-models to redefine normalization as the flux within the 0.3–7.0 keV band. With this definition, flux errors could be obtained trivially without correlations between different fit parameters biasing our results. For most sources the data were consistent with the co-added spectrum, although several of the brighter objects required additional N_H and in two cases we found an appreciably softer spectrum. Whilst this method preferentially corrects the brightest sources, only in a few cases was there a dramatic change in the L_X . Considering the large luminosity errors of the faintest sources, this is unlikely to bias our results substantially.

In order to compare more directly with other authors, we additionally computed counts-to-flux conversion factors for each of our sources. To allow for effective-area variations between detections, we folded the best-fit composite source *bremssstrahlung* model ($N_H=0.02 \times 10^{22} \text{cm}^{-2}$, $kT=8 \text{ keV}$) through the instrumental responses of each source to determine a local counts-to-flux conversion factor. The Poissonian errors upon the measured counts were estimated using the Gehrels’ approximation and translated into flux errors. We found excellent agreement between both methods of flux estimation, except in a few sources which showed unusually absorbed spectra. The results of our flux estimation are shown in Table 1, which also defines our source naming convention (sources being numbered in descending order of luminosity).

For the distance to NGC 1332 (23 Mpc), we found that 8 sources have $L_X > 10^{39} \text{ erg s}^{-1}$, which qualifies them as ULX. The expected number of bright background objects in this sample is, however, appreciable (4, based on the Chandra deep field observations; Sect. 5), so some are

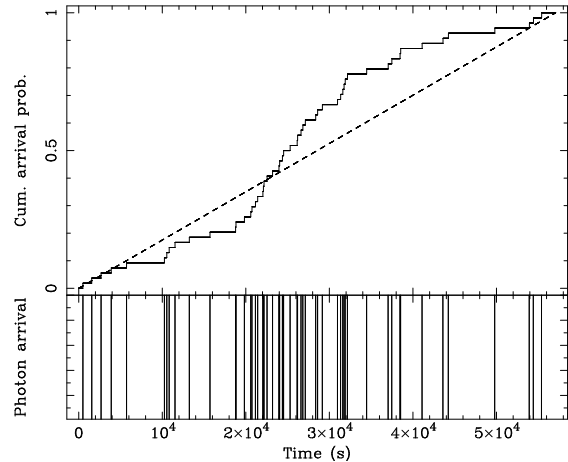


FIG. 4.— Full energy-band “lightcurve” of the variable source 51. Since so few photons were detected, we adopt a non-standard way of showing the lightcurve. In the lower panel, each arriving photon is flagged as a vertical line, whereas the upper panel shows a comparison between the measured cumulative arrival probability of the photons in the source (solid line) and that expected for a non-varying source (dashed line)

undoubtedly background objects. In order to compare with other authors, we considered separately only those ULX within the D_{25} region, of which there are 2, with an expected background number of 0.3. Neither of these sources has $L_X > 2 \times 10^{39} \text{ erg s}^{-1}$.

4.4. Variability

To search for variability we accumulated source and background lightcurves with the maximum temporal resolution (3.24 s) for each source. Since the time binning was very fine ($T_{\text{bin}} \ll T_{\text{exp}}$), we were able to compare the observed distribution of photon arrival times with that expected for a non-varying source, using the Kolmogorov-Smirnov (K-S) test (which requires *unbinned* data). The K-S test is fairly sensitive to large-amplitude variability occurring over timescales comparable to T_{exp} . To minimize false positive detections, since we were considering a total of 74 sources (including the point-source in NGC 1331), we required that the null hypothesis (no variability) be rejected at 99.93% significance (corresponding to a 5% probability of a single false positive).

We found that, of our sources, only two were variable at the required significance (as indicated in Table 1). Since the background is known not to be entirely constant (due to flaring), we tested these lightcurves having excluded flaring and found a comparably strong detection of variability. In addition, we further tested the entire locally-accumulated background lightcurves of these sources using the same test. In neither case could the null hypothesis (no variability in the background) be rejected at better than 7% significance. It is therefore highly improbable that the measured variability of the sources arises from background fluctuations. Considering only the sources within the D_{25} region (and consequently lowering our detection significance threshold) did not lead to any further detections of variability. Both variable sources had luminosities $\sim 1\text{--}3 \times 10^{38} \text{ erg s}^{-1}$, comparable to the Galactic “Z-track” sources, which can show variability

over similar time-scales (Hasinger & van der Klis 1989). There were too few photons from each source, however, to classify these objects definitively. This will require a more sensitive, long-term study to track the spectral and timing behaviour.

4.5. Spatial extent and the search for a central source

The detection algorithm is capable of identifying both point-like and extended sources. In order to identify any sources which may be extended, we examined the radial brightness profiles accumulated for each source. Fitting was performed using dedicated software which was able to make use of the radial profiles described in Sect. 3 and to take account of the instrumental point-spread at the peak photon energy of each source. The source data were rebinned into ~ 90 logarithmically-spaced radial bins and then adjacent bins were regrouped to ensure none contained fewer than 20 photons. The data were initially fitted with a model comprising a constant background term and a point-source at the extraction centroid. To account for exposure variation over the S3 chip, an exposure-map was generated for the source image at 1.7 keV and used to correct the applied model. For those sources within $\sim 0.5'$ of the galaxy centroid, the substantial diffuse emission contaminated the profile sufficiently that a constant background model was no longer tenable. In these cases, we included an additional component, corresponding to a β -model (with parameters matching the diffuse galactic emission; Paper III) and centred at an appropriate distance from the point-source.

In all except one case we found no evidence of spatial extent greater than the instrumental PSF, placing limits of ~ 50 – 100 pc (depending on the position in the field-of-view) on the actual size of these objects. Fig. 5 shows the results for Source 14, which is clearly more extended than the PSF. Replacing the point-source with a β -model improved the χ^2/dof from 104/60 to 59/58, which is significant at $> 99.999\%$ (upon the basis of an f-test). We were also able to fit the radial profile as two point-sources, one centred at the extraction centroid and one $1.0_{-0.06}^{+0.4}''$ away from it, of approximately equal brightness. Since we might expect two sources this far apart to be distinguishable by *Chandra*, we tested this conclusion by simulating an image of two-point sources (separated by $1''$) at an equivalent position in the focal-plane (generating 1.0 keV point-source images from the *Caldb* PSF hypercubes). If there were more than ~ 100 counts in the sources they could be resolved. When we reduced the number of photons to ~ 25 each (corresponding to the observed number of counts in Source 14), Poisson noise blurred the outlines so that they remained unresolved. This is a practical example of source-confusion. The probability of a chance alignment of a background object within $1''$ of one of our detected sources was, however, only $\sim 1\%$. Such a low probability does tend to suggest that the source was genuinely extended (having a size $\sim 1''$), although we cannot altogether rule out the possibility of a chance superposition. Future observations may be able to resolve the issue by identifying variability in this source, which would place limits on its size.

In addition, we searched for a point-source embedded in the diffuse emission at the galactic centre. The radial profile of the diffuse emission out to $4.2'$ was grouped into ~ 150 logarithmically-spaced bins. These

were regrouped to ensure at least 20 photons in each bin. The data could be well-approximated with a single β -model plus a constant background term (folding in the instrumental PSF at 1.0 keV and correcting the model for exposure variations and gaps arising from removed point-sources), as shown in Fig. 5. Although the profile is extremely peaked ($R_{\text{core}} = 1.2 \pm 0.1''$) its centre is significantly broader than the PSF of *ACIS* at its position. Adding a central point-source model does not improve the fit quality, placing an upper limit of $13.4 \times 10^{-4} \text{ count s}^{-1}$ ($L_X < 8.4 \times 10^{38} \text{ erg s}^{-1}$) on any central source. A more detailed discussion of the morphology and radial profile of the diffuse emission will be given in Paper III.

4.6. Source identification

In order to identify possible counterparts to the point-sources we checked for objects listed in *NED*, Simbad and the Tycho-2 catalogue of Galactic (foreground) stars (Høg et al. 2000) within $2''$ of each source. We did not identify any obvious counterparts to X-ray sources which would enable us independently to check the absolute astrometry. However, the centroid of the diffuse galactic emission of NGC 1332 was located within $1''$ of the 2MASS galaxy centroid (listed in *NED*), which is accurate to $\sim 2''$ and there are no known pointing problems reported for our *Chandra* data. Therefore, we assumed that the astrometry of the detected sources was accurate to $2''$. Only one counterpart was found to any source, that being NGC 1331, the centroid of which lies within $1''$ of an X-ray source (which we have not listed in Table 1).

In addition, we checked for coincidence between the point source positions and a list of GC candidates kindly supplied by A. Kundu (priv. comm.). The GC candidates were identified in HST WFPC2 observations centred on NGC 1332 (Kundu & Whitmore 2001), which encloses only $\sim 50\%$ of the D_{25} region. In order to perform this comparison it was necessary to check the relative astrometry between *Chandra* and HST. A comparison of the X-ray centroid and the optical centre in the appropriate archival WFPC2 image clearly revealed a systematic offset of $\sim 1.6''$ between *Chandra* and HST. Compensating for this effect, we found that 9 sources lay within $0.75''$ of a GC candidate and so we assumed they were associated with a globular cluster. We adopted this limit since it corresponded to an apparent break in the distribution of offsets between GC and the X-ray source positions. A total of 30 X-ray sources coincided with the WFPC field-of-view (of which 23 were within D_{25}), and there were a total of 204 GC candidates in this region of NGC 1332, so that $\sim 30\%$ of the X-ray sources within this region were identified with GCs and 4.4% of all GCs hosted LMXB. Both of these results are consistent with observations of other early-type galaxies (Kundu et al. 2002; Sarazin et al. 2003, e.g.). We investigated whether there was any evidence of a systematic difference in the luminosities of the GC and the non-GC sources by comparing the fluxes of the two populations using a two-sample Kolmogorov-Smirnov test. We found no evidence of a statistically significant discrepancy between the two distributions, which agreed with $\sim 60\%$ probability. The combined spectra of the GC sources exhibited no evidence of a systematic difference from the other sources.

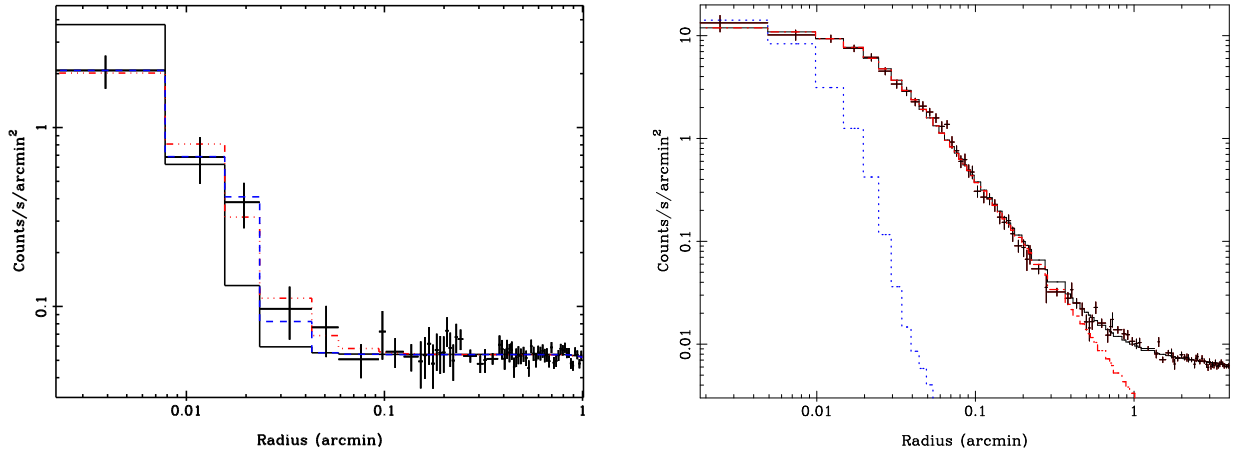


FIG. 5.— Left panel: Full energy-band radial brightness profile for source 14. Three fits to the radial brightness profile are also shown. These comprise a constant background term and, respectively, the expected satellite point-spread computed at the peak source energy of 1.3 keV (solid line), a beta-model (dash-dotted line) and a pair of point-sources separated by $1''$ (dashed line). Right panel: radial brightness profile of the diffuse central emission from 0.3–7.0 keV. The data are shown with a fit comprising a constant background term plus a simple β -model. The β -model component is also shown separately (dash-dot line), and, for comparison, the azimuthally-averaged PSF (dotted line). There is no evidence of a central point-source.

4.7. Spatial distribution of sources

We examined the spatial distribution of the point-sources in order to determine to what extent they may follow either the optical light or the X-ray surface-brightness of the gas. In order to do this, we initially accumulated a histogram of the number of sources within each of 128 evenly-spaced radial bins centred at the galaxy centroid, and excluding the inner $\sim 0.2'$ (where source detection incompleteness is most severe). In order to improve the signal-to-noise level, the data were rebinned until each bin contained at least 5 sources. Models were tested against the data using the Cash-statistic (the goodness-of-fit being determined by Monte-Carlo simulation). We also tried using the χ^2 statistic (which was less rigorous due to the low count-statistics) and obtained comparable results. We tested two different models against the data, one following the optical light of the galaxy and one following the X-ray contours. To approximate the optical profile it was convenient to fit a single de Vaucouleurs profile with its effective radius fixed to $31''$. We chose this value by correcting the semi-major axis effective radius measured by BC to account for the fact that our data were azimuthally averaged and not corrected for ellipticity. In addition, we tested a simple β -model, with a shape matching that of the diffuse emission, against the data. In both cases, we added an additional (constant) term to account for unrelated “background” sources. We were able to obtain good fits to the data with both models (null hypothesis probabilities of 56% and 28%, respectively), for which the inferred numbers of background sources agreed within errors. Fig 6 shows the data and the best-fit de Vaucouleurs model. For our de Vaucouleurs fit, we found a total of 1300_{-800}^{+1000} background sources per degree, equivalent to a total of $1.9_{-1.2}^{+1.5}$ background sources in the D_{25} region. Taking our lowest measured flux to be the completeness limit, we would expect, (based upon the number of sources detected by Tozzi et al. 2001 in the Chandra Deep Field image), there to be between ~ 1400 and ~ 2600 sources per degree (for the “soft” and “hard” bands of these au-

thors, corrected to our 0.3–7.0 keV band). Our data were clearly, therefore, in general agreement with the expected number of background sources from these observations.

In addition, we accumulated a histogram of the azimuthal source distribution. We binned the data into 128 azimuthal bins, regrouping adjacent bins until there were at least 5 sources in each. We considered only sources within $2'$ of the galaxy centroid to minimize background-source contamination. Models were tested against the data using the Cash statistic, exactly as for the radially-binned data. The data clearly showed azimuthal variation, as would be expected if the sources follow the optical light. Formally, we found that a model in which the source density is constant with angle gives a null hypothesis only of 1.8% and therefore was rejected. Alternatively, for a model in which the number of sources followed the optical light, the null hypothesis probability of 70% indicated excellent agreement with the data (see Fig 6).

4.8. Source completeness estimate

A number of factors can influence the likelihood of detecting a given point source, such as source confusion in crowded regions, increased local background due to diffuse emission and the degradation of the *Chandra* point-spread off-axis. The importance of correcting the measured XLF to account for incompleteness was demonstrated by Kim & Fabbiano (2003b), who showed that failure to account for it can lend erroneous significance to XLF breaks. In order to estimate the level of incompleteness in our source detections we adopted a technique similar to that outlined by Kim & Fabbiano (2003b). We ran a large number of Monte-Carlo simulations in which a small number of sources were added to the *observed* image of NGC 1332 in the 0.1–10 keV band and then measured the fraction of these sources which could be found with the detection algorithm. Since our adoption of additional energy-bands did not appreciably add to the number of detected sources, it was appropriate to consider only the 0.1–10 keV energy-band in this calculation. The added sources were all assumed to have

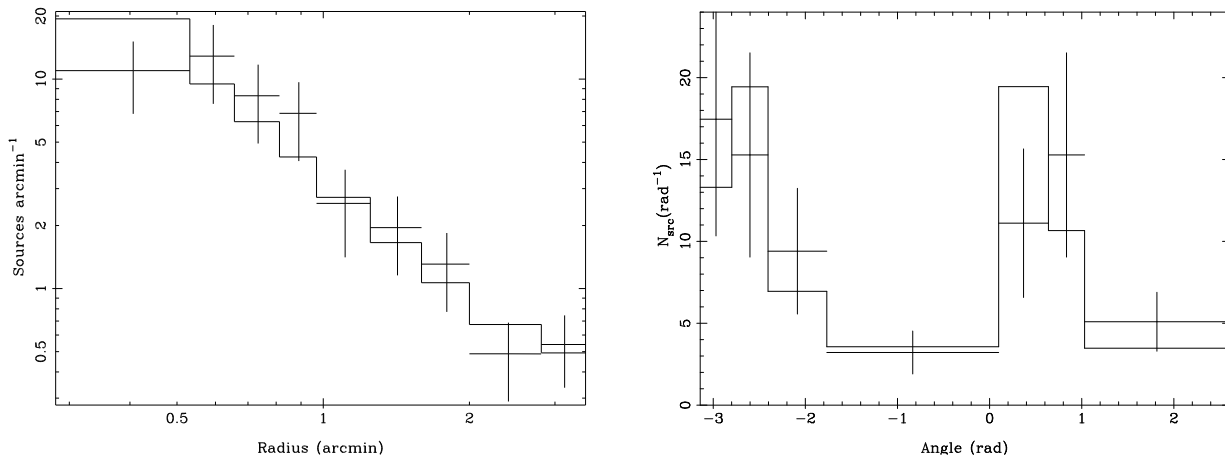


FIG. 6.— Left panel: The radial distribution of the point-sources, binned to ensure at least 5 sources per bin and shown with the best-fit model following the optical light. Right panel: The azimuthal distribution of sources, shown with the best-fit model, which also follows the optical light.

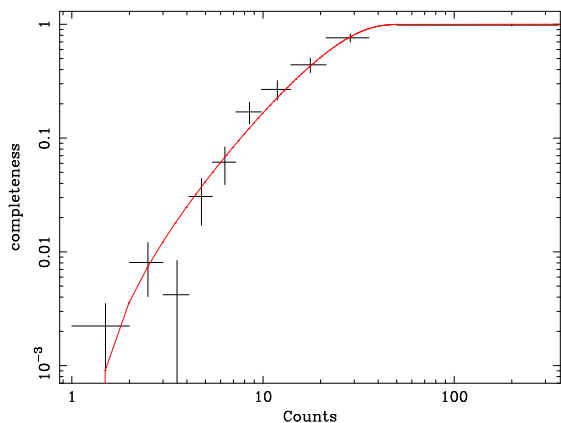


FIG. 7.— Representative plot of the detection probability for a point-source at a given luminosity as a function of measured counts. Also shown is our polynomial approximation to the function.

spectra which were strongly peaked at 1 keV and appropriate images were extracted from the *Caldb* PSF hypercube and added to the image (having been degraded with suitable Poisson noise). The sources were added with an assumed luminosity function, $(dN/dS)_0 \propto S^{-2}$ (although its adopted shape does not affect the results) and, in order to speed the computation, we added ~ 10 sources at a time to each image down to a limiting flux of 1 count per image. These were assumed to be distributed as the optical light (i.e. an elliptical de-Vaucouleurs profile with axis ratio and alignment matching that of the D_{25} ellipse and with major-axis $0.55''$; BC). Although ideally sources would be added one-at-a-time so as not to introduce any biases, this expedient is not strictly necessary provided the incidence of overlap between added sources is low. After a total of 400 simulations, we were able to measure the function $P_d(S)$, which is the probability that a source with *exactly* S counts is detected. Due to the finite number of test sources, we binned them into a number of \sim logarithmically-spaced luminosity-bins and computed the fraction of sources detected within each bin (Fig 7). $P_d(S)$ is given by the ratio of the measured and simulated differential XLF. We were then able to

approximate $P_d(S)$ by a fourth-order polynomial in the range $S=1-50$ counts (also shown in Fig 7). We considered only simulated sources lying within the D_{25} ellipse, since we later computed the XLF only in this region.

5. THE X-RAY LUMINOSITY FUNCTION

In order to minimize the possible impact of background source contamination (a strong source of potential error given field-to-field variations in the number of background objects), when computing the XLF we considered only those sources within the D_{25} region. We fitted the differential luminosity function, separately considering the XLF derived from our two different flux-estimation techniques. Accordingly, the sources were binned as a function of luminosity in such a way that the bin size increased geometrically (progressively scaling by a factor 2.0). We experimented with different scaling factors but found our results were relatively insensitive to the adopted binning. Since our measurement included no upper luminosity cut-off, it is significant that we detected no sources with luminosities greater than $\sim 12 \times 10^{38}$ erg s^{-1} . Therefore, an additional data-bin containing zero sources and covering an extremely wide luminosity range (from $L_X \simeq 12-10000 \times 10^{38}$ erg s^{-1}) was added to our data (the fit statistic is extremely insensitive to the precise upper bound of this bin, provided it is larger than $\sim 100 \times 10^{38}$ erg s^{-1}). Including this bin leads to steeper XLF fits than omitting it. To fit the XLF we minimized the Cash statistic since our data were dominated by Poisson errors. The fit quality of the model was subsequently determine *via* Monte-Carlo simulations. To take account of flux measurement errors, we repeated the fit 100 times for each model, having first added appropriate Gaussian noise to the measured L_X of each source. If any resulting L_X would be below our lowest measured luminosity (assumed to be the source detection limit), it was recomputed. In order to test the reliability of this fitting procedure, we simulated 100 luminosity functions from our best-fit model and attempted to recover the best-fit parameters. We found good agreement between the inferred and expected results and confirmed the expected statistical scatter, giving us confidence in our ability to determine parameters and estimate error-

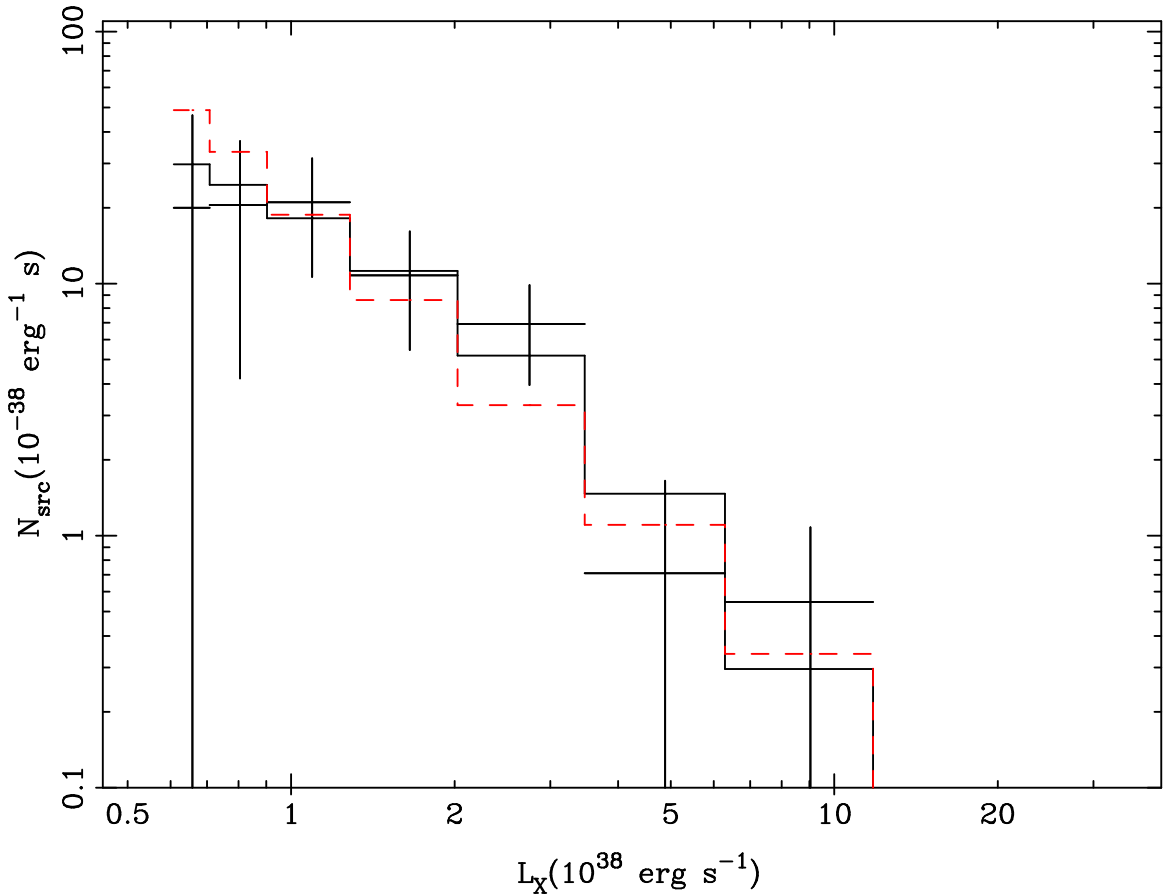


FIG. 8.— The *differential* luminosity-function of the data. Error-bars, estimated from the Gehrels’ approximation, have been included on each point only as a guide to the eye since the Cash statistic was used in fitting. Also shown are the best-fit completeness-corrected power law model (solid line) and with the best-fit uncorrected simple power law model (dashed line). This demonstrates the impact of incompleteness on measuring the XLF.

bars reliably, provided the simulations were representative, which we believe.

We tested a number of models against the data, in each case adding a separate component to account for the point-source population due to background sources. This term had a power law shape, i.e.

$$\frac{dN}{dL} = K \left(\frac{L_X}{10^{38} \text{ erg s}^{-1}} \right)^{-\beta} \quad (1)$$

We fixed the slope, β , and the amplitude, K , to values consistent with the hard-band sources of Tozzi et al. (2001), i.e. 1.92 and 2.1 sources per $10^{38} \text{ erg s}^{-1}$, respectively (correcting fluxes from the 2.0–10.0 keV band used by these authors to our 0.3–7.0 keV band). This term did not contribute very significantly to our fit and corresponds to ~ 3.5 sources in total in the D_{25} region. We found that allowing the normalization to be free, or adopting the shape and normalization appropriate for the soft band of Tozzi et al. (2001) made little difference to our overall fit. Without applying any form of completeness correction to our data, we found that a single power law fit (with fluxes estimated from spectral-fitting) gave a very poor fit to the data (having a null hypothesis probability of 0.3%). Adding a break in the model at $L_{\text{break}} = 2.3_{-0.7}^{+1.4} \times 10^{38} \text{ erg s}^{-1}$ substantially improved the fit quality (giving a null hypothesis probability of 42%), although the power law slopes were

poorly-constrained (e.g. $\beta = 2.6_{-0.7}^{+1.3}$ for $L_X > L_{\text{break}}$). To correct for source detection incompleteness we modified the simple power law by multiplication with our completeness estimate function (i.e. we corrected the *model* rather than the data, to allow us to continue using Poisson statistics). We obtained an excellent fit with the corrected single power law model (the null hypothesis probability now being 40%). The best-fit parameters were $\beta = 2.3 \pm 0.4$ and amplitude, $K = 60 \pm 25$, and no break was required. This indicates that incompleteness was responsible for the break measured in the uncorrected data. No further improvement in the fit could be obtained by adding a break to the power law model, and the resulting fit-parameters were very poorly-constrained. The measured value of β was in good agreement with that obtained by Kim & Fabbiano (2003b) for a sample of 14 early-type galaxies. However, these authors computed source fluxes based on a counts-to-flux conversion, so this is not strictly a fair comparison.

We separately considered the XLF where fluxes were obtained from the count-rate, rather than the spectra. This allowed us to compare our results more directly with other authors, who tend to adopt this procedure. Exactly as above, we found that a broken power law gave a much better fit than a simple power law to the data, but this effect vanished when proper account is made for the source detection incompleteness. In this case, however,

we obtained a somewhat steeper slope for our luminosity-function ($\beta = 2.7 \pm 0.5$; K was correspondingly altered to 87 ± 33), although the two β values agree within errors. The differential XLF and the best-fit model are shown in Fig. 8, along with the uncorrected single power law fit. It is not surprising that the XLF derived from fitting the spectra was less steep, since the principal effect of the fitting was to uncover sources with more than Galactic N_{H} , thereby populating more the higher luminosities. Since some of these “absorbed” sources may have been background AGN and since the background XLF we adopted were computed from *counts-to-flux* conversion, it is probably more correct to adopt our $\beta = 2.7 \pm 0.5$ result. Intriguingly, this result is marginally ($\sim 2.5\sigma$) steeper than the $\beta = 2.0$ value found by Kim & Fabbiano (2003b) but is in good agreement with their higher-luminosity slope when they fitted a broken power law to the combined, incompleteness-corrected XLF. To verify that our slope was not biased by our use of data during the mild flaring, we recomputed all fluxes having excised data during the flares. The slope of the XLF was unchanged.

As a final note, we also attempted to fit the XLF using two alternative fitting methods: a maximum-likelihood method appropriate for unbinned data (Crawford et al. 1970) and minimization of the Kolmogorov-Smirnov (K-S) test statistic. In both cases we obtained less stringent constraints than for our binned-data analysis above. Since, by its nature, the K-S test is relatively insensitive at the sparsely-populated highest and lowest luminosities, that statistic in particular was much less reliable at determining the quality of the fit.

6. DISCUSSION

We have found a total of 73 point-sources within the *Chandra* S3 field of NGC 1332, including 37 which lie within the D_{25} isophote and none of which is coincident with the galaxy centroid. We expect a total of $1.9^{+1.5}_{-1.2}$ unrelated background or foreground sources to be within D_{25} , so that the vast majority of these sources are associated with the galaxy. The spatial distribution of the sources was consistent with the optical isophotes, as may be expected from a population of sources of stellar origin which has not been recently disturbed by merger activity (Zezas et al. 2003). In total 30% of the X-ray sources were associated with globular clusters, and 4.4% of GCs contained an X-ray source, both of which results are consistent with other early-type galaxies. The phenomenology of the individual sources was consistent with expectations for an LMXB population. Two sources had soft spectra, consistent with high-state black-hole binaries and two sources were variable during the observation. Intriguingly one source was extended, although its radial profile was consistent with two unresolved point-sources.

Without taking into account the impact of source detection incompleteness at the lowest luminosities (where source confusion and increased background due to diffuse gas reduce the probability of detecting a source), we found that the XLF of the point-sources within D_{25} can be fitted by a power law with a break at $L_{\text{X}} \sim 2 \times 10^{38} \text{ erg s}^{-1}$. Similar results have been reported in other early-type galaxies (e.g. Sarazin et al. 2001; Blanton et al. 2001). However, when we made corrections for the expected level of incompleteness, we found that the data were extremely well-fitted by a sin-

gle power law, with a differential slope, $\beta = 2.7 \pm 0.5$. Assuming that the XLF remains unbroken down to $10^{37} \text{ erg s}^{-1}$ (as seen for sources in M 31: Kong et al. 2002), we estimate a total luminosity of $180 \pm 70 \times 10^{38} \text{ erg s}^{-1}$ due to *unresolved* point-sources in the D_{25} region. Comparing this to the B-band luminosity of the galaxy, obtained from the face-on, extinction-corrected B-band luminosity listed in the *LEDA*⁴ catalogue, we obtained $L_{\text{LMXB}}/L_{\text{B}} = 0.8 \pm 0.3 \times 10^{30} \text{ erg s}^{-1} L_{\text{B}\odot}^{-1}$. In addition, we compared with the K-band luminosity (adopting the K_{20} magnitude obtained by 2MASS), and obtained $L_{\text{LMXB}}/L_{\text{K}} = 0.13 \pm 0.05 \times 10^{30} \text{ erg s}^{-1} L_{\text{K}\odot}^{-1}$. Both of these values were in excellent agreement with observations of other early-type galaxies (Kim & Fabbiano 2003b).

The slope of our XLF fit closely resembles that found at high luminosities in a variety of other early-type galaxies (Sarazin et al. 2001; Blanton et al. 2001; Colbert et al. 2003). A slope of $\beta \simeq 2.7$ is also strikingly similar to observations of a primarily old stellar population in M31, but which does not extend to such high luminosities (Kong et al. 2003). The slope is, however, marginally ($\sim 2.5\sigma$) steeper than the incompleteness-corrected *single* power law fits found in a recent survey of early-type galaxies (Kim & Fabbiano 2003b). Intriguingly, these authors reported some evidence of a break at $\sim 5 \times 10^{38} \text{ erg s}^{-1}$, above which $\beta \simeq 2.7$ is observed. A similar result has also been found for M84 (Finoguenov & Jones 2002). A break at this luminosity should be observable within our data, and its apparent absence is intriguing. Whilst it is certainly true that *statistically* acceptable single power law fits were found for most galaxies in the sample of Kim & Fabbiano (2003b), the resulting slope ($\beta \simeq 2.0$) may simply be an “average” of the slopes above and below the break. The steep slope seen in NGC 1332 might therefore suggest that such a break is absent in this galaxy. It must be stressed, however, that there are some differences in the analysis procedures adopted by these authors and those used in the present work, which may simply weight our fit somewhat more heavily towards the high luminosity sources (especially our inclusion of a high-luminosity, unoccupied bin). Due to the small numbers of sources, however, the error-bars on the best-fit slope in NGC 1332 are large, so that the disagreement is only at $\sim 2.5\sigma$. It remains to be seen whether comparable results are observed in any other galaxies containing significantly more X-ray point sources. Nonetheless, if the absence of the break in our XLF is confirmed, it is an interesting result, which casts further doubt on there being a “universal” break in early-type galaxies corresponding to the division between neutron-star and black-hole binary systems.

The origin of the XLF break is still somewhat unclear. Although it was originally suggested that a break might mark the division between neutron-star and black-hole binary systems (Sarazin et al. 2001), the disparity between the reported break luminosities in several galaxies and the Eddington limit for a $1.4M_{\odot}$ (canonical) neutron-star suggests another origin, perhaps in the star-formation history of the galaxy (e.g. Jeltrema et al. 2003; Wu 2001). In that case, however, we might expect to see a strong correlation between the age of the sys-

⁴ <http://leda.univ-lyon1.fr/>

tem (since the last major merger) and the XLF shape; comparing the slopes found by Kim & Fabbiano (2003b), including that for NGC 720, and galaxy ages given by Terlevich & Forbes (2002) we find no evidence of a correlation. However, this includes only 8 sources and will need to be confirmed with a larger sample.

We detected two ULX within the D₂₅ region of NGC 1332, although neither of these sources have $L_X > 2 \times 10^{39}$ erg s⁻¹. Such numbers are consistent with other galaxies of similar morphology (Humphrey et al. 2003). The unbroken XLF of late-type galaxies suggests that the ULX associated with star-formation can be attributed to the high-luminosity tail of the HMXB XLF, which is flatter than the LMXB XLF (Grimm et al. 2003). It may be that, in a similar way, the ULX in early-type galaxies simply represent the high- L_X tail of the LMXB XLF. Irwin et al. (2003b) have argued that sources with $L_X > 2 \times 10^{39}$ erg s⁻¹ are extremely rare in early-type galaxies, suggesting that the most luminous ULX may therefore represent a population almost entirely alien to such galaxies. However luminous ULX have been reported in NGC 1399 and NGC 720 which are associated with GCs (hence unlikely to be background objects; Angelini et al. 2001; Jeltama et al. 2003), so they are clearly not entirely absent and therefore it is of interest to determine if their paucity simply reflects the steepness of the XLF. In NGC 1332, since our fitting took account of the absence of sources at high luminosities, the absence of very luminous ULX is consistent with the high-luminosity tail of the XLF. However, we also compared the ratio of the number of sources measured by Irwin et al. (2003b) in the $1-2 \times 10^{39}$ erg s⁻¹ and the

$> 2 \times 10^{39}$ band, to that expected assuming our best-fit XLF slope ($\beta = 2.7$). We found a likelihood of $\sim 1\%$ of reproducing the data from the model, although allowing β to steepen within its error-bars increased the likelihood to $\sim 5\%$. Nonetheless this suggests the possibility of a change in the XLF at $\sim 1-2 \times 10^{39}$ erg s⁻¹. Intriguingly, an XLF break was reported by Jeltama et al. (2003) around this luminosity.

The authors would like to thank Claude Canizares for helpful discussions and carefully reading the manuscript. We would like to thank Arunav Kundu for very kindly supplying the list of GC candidates. We would also like to thank Aaron Lewis for helpful discussions concerning *Chandra* analysis. This research has made use of the NASA/IPAC Extragalactic Database (*NED*) which is operated by the Jet Propulsion Laboratory, California Institute of Technology, under contract with the National Aeronautics and Space Administration. This research also made use of the SIMBAD database, operated at CDS, Strasbourg, France. In addition we used the LEDA on-line galaxy database. Support for this work was provided by NASA through *Chandra* award number G02-3104X, issued by the Chandra X-ray Observatory Center, which is operated by the Smithsonian Astrophysical Observatory for and on behalf of NASA under contract NAS8-39073. Partial support for this work was also provided by NASA under grant NAG5-13059, issued through the Office of Space Science Astrophysics Data Program.

REFERENCES

- Angelini, L., Loewenstein, M., & Mushotzky, R. F. 2001, *ApJ*, 557, L35
- Belczynski, K., Kalogera, V., Zezas, A., & Fabbiano, G. 2003, *ApJ*, in press, astro-ph/0310200
- Blanton, E. L., Sarazin, C. L., & Irwin, J. A. 2001, *ApJ*, 552, 106
- Brown, B. A. & Bregman, J. N. 2001, *ApJ*, 547, 154
- Buote, D. A. & Canizares, C. R. 1996, *ApJ*, 457, 177
- Buote, D. A. & Canizares, C. R. 1997, *ApJ*, 474, 650
- Buote, D. A., Humphrey, P. J., & Canizares, C. R. 2004, in preparation. (Paper III)
- Church, M. J. & Bałucińska-Church, M. 2001, *A&A*, 369, 915
- Colbert, E., Heckman, T., Ptak, A., & Strickland, D. 2003, *ApJ*, in press, astro-ph/0305476
- Colbert, E. J. M. & Mushotzky, R. F. 1999, *ApJ*, 519, 89
- Colbert, E. J. M. & Ptak, A. F. 2002, *ApJS*, 143, 25
- Crawford, D. F., Jauncey, D. L., & Murdoch, H. S. 1970, *ApJ*, 162, 405
- Davis, D. S. & Mushotzky, R. F. 2003, *ApJ*, in press, astro-ph/0312211
- de Vaucouleurs, G., de Vaucouleurs, A., Corwin, H. G., Buta, R. J., Paturel, G., & Fouque, P. 1991, *Third Reference Catalogue of Bright Galaxies (Volume 1-3, XII, 2069 pp. 7 figs.. Springer-Verlag Berlin Heidelberg New York)*
- Dickey, J. M. & Lockman, F. J. 1990, *ARA&A*, 28, 215
- DiStefano, R. & Kong, A. 2003, *ApJ*, submitted, astro-ph/0311374
- Fabbiano, G. 1989, *ARA&A*, 27, 87
- Fabbiano, G. & White, N. E. 2003, in *Compact Stellar X-ray Sources*, ed. W. H. G. Lewin & M. van der Klis (C.U.P.), astro-ph/0307077
- Finoguenov, A. & Jones, C. 2002, *ApJ*, 574, 754
- Freeman, P. E., Kashyap, V., Rosner, R., & Lamb, D. Q. 2002, *ApJS*, 138, 185
- Grimm, H.-J., Gilfanov, M., & Sunyaev, R. 2003, *MNRAS*, 339, 793
- Hasinger, G. & van der Klis, M. 1989, *A&A*, 225, 79
- Høg, E., Fabricius, C., Makarov, V. V., Urban, S., Corbin, T., Wycoff, G., Bastian, U., Schwekendiek, P., & Wicenec, A. 2000, *A&A*, 355, L27
- Humphrey, P. J., Buote, D. A., & Canizares, C. R. 2004, in preparation. (Paper II)
- Humphrey, P. J., Fabbiano, G., Elvis, M., Church, M. J., & Bałucińska-Church, M. 2003, *MNRAS*, 344, 134
- Irwin, J. A., Athey, A. E., & Bregman, J. N. 2003a, *ApJ*, 587, 356
- Irwin, J. A., Bregman, J. N., & Athey, A. E. 2003b, *ApJ*, in press, astro-ph/0312393
- Jeltama, T. E., Canizares, C. R., Buote, D. A., & Garmire, G. P. 2003, *ApJ*, 585, 756
- Kilgard, R. E., Kaaret, P., Krauss, M. I., Prestwich, A. H., Raley, M. T., & Zezas, A. 2002, *ApJ*, 573, 138
- Kim, D. & Fabbiano, G. 2003a, *ApJ*, 586, 826
- Kim, D.-W. & Fabbiano, G. 2003b, *ApJ*, submitted, astro-ph/0312104
- Kim, D.-W., Fabbiano, G., & Trinchieri, G. 1992, *ApJS*, 80, 645
- King, A. R. 2002, *MNRAS*, 335, L13
- King, A. R., Davies, M. B., Ward, M. J., Fabbiano, G., & Elvis, M. 2001, *ApJ*, 552, L109
- Kong, A. K. H., DiStefano, R., Garcia, M. R., & Greiner, J. 2003, *ApJ*, 585, 298
- Kong, A. K. H., Garcia, M. R., Primini, F. A., Murray, S. S., DiStefano, R., & McClintock, J. E. 2002, *ApJ*, 577, 738
- Kraft, R. P., Kregenow, J. M., Forman, W. R., Jones, C., & Murray, S. S. 2001, *ApJ*, 560, 675
- Kundu, A., Maccarone, T. J., & Zepf, S. E. 2002, *ApJ*, 574, L5
- Kundu, A., Maccarone, T. J., Zepf, S. E., & Puzia, T. H. 2003, *ApJ*, 589, L81
- Kundu, A. & Whitmore, B. C. 2001, *AJ*, 122, 1251
- Makishima, K., et al. 2000, *ApJ*, 535, 632
- Matsushita, K., et al. 1994, *ApJ*, 436, L41
- Paczyński, B. 1983, *ApJ*, 267, 315
- Roberts, T. P. & Warwick, R. S. 2000, *MNRAS*, 315, 98
- Sarazin, C. L., Irwin, J. A., & Bregman, J. N. 2001, *ApJ*, 556, 533

- Sarazin, C. L., Kundu, A., Irwin, J. A., Sivakoff, G. R., Blanton, E. L., & Randall, S. W. 2003, *ApJ*, 595, 743
- Saviane, I., Hibbard, J. E., & Rich, R. M. 2003, *ApJ*, in press, astro-ph/0311200
- Terlevich, A. I. & Forbes, D. A. 2002, *MNRAS*, 330, 547
- Tonry, J. L., Dressler, A., Blakeslee, J. P., Ajhar, E. A., Fletcher, A. ., Luppino, G. A., Metzger, M. R., & Moore, C. B. 2001, *ApJ*, 546, 681
- Tozzi, P., et al. 2001, *ApJ*, 562, 42
- White, N. E. & Marshall, F. E. 1984, *ApJ*, 281, 354
- White, N. E., Nagase, F., & Parmar, A. N. 1995, in *X-ray Binaries*, ed. W. H. G. Lewin, J. van Paradijs, & E. P. J. van den Heuvel (C.U.P.), 1-57
- Wu, K. 2001, *Publications of the Astronomical Society of Australia*, 18, 443
- Zezas, A. & Fabbiano, G. 2002, *ApJ*, 577, 726
- Zezas, A., Fabbiano, G., Rots, A. H., & Murray, S. S. 2002, *ApJS*, 142, 239
- Zezas, A., Hernquist, L., Fabbiano, G., & Miller, J. 2003, *ApJ*, in press, astro-ph/0310567

TABLE 1
SOURCES DETECTED

Src	Name	Rate (10^{-4} s^{-1})	L_X^{spec} ($10^{38} \text{ erg s}^{-1}$)	L_X^{rate} ($10^{38} \text{ erg s}^{-1}$)	ΔR (l)	In D ₂₅	Comment
1	CXOU J032636.5-211809	81.	$58. \pm 5.$	$60. \pm 5.$	4.9	no	R
2	CXOU J032614.8-212126	95.	$53. \pm 4.$	$46. \pm 3.$	1.4	no	A, R, NG
3	CXOU J032604.4-212258	45.	$36. \pm 5.$	$24. \pm 3.$	4.1	no	A
4	CXOU J032620.7-212151	11.	$23._{-3.}^{+9.}$	5.3 ± 1.3	1.9	no	A, NG
5	CXOU J032632.8-212306	6.0	$12._{-3.}^{+4.}$	8.6 ± 3.6	4.7	no	A, C
6	CXOU J032618.1-212014	18.	$12._{-2.}^{+3.}$	$12. \pm 2.$	0.23	yes	A, B, R, NG
7	CXOU J032601.7-211726	21.	$12. \pm 2.$	$12. \pm 2.$	4.5	no	
8	CXOU J032616.7-211954	19.	$12. \pm 2.$	$11. \pm 2.$	0.26	yes	NG
9	CXOU J032618.7-212031	17.	7.8 ± 1.8	8.4 ± 1.6	0.51	yes	NG
10	CXOU J032606.8-212016	12.	$7.2_{-1.3}^{+2.0}$	6.1 ± 1.4	2.4	no	
11	CXOU J032616.9-212006	8.8	6.7 ± 2.6	5.3 ± 2.3	0.094	yes	NG
12	CXOU J032612.5-212342	6.2	$6.6_{-1.8}^{+2.1}$	3.3 ± 1.2	3.7	no	A
13	CXOU J032609.7-212211	9.1	5.9 ± 1.9	4.6 ± 1.3	2.7	no	
14	CXOU J032614.6-211903	10.	5.8 ± 1.6	5.2 ± 1.3	1.2	no	E
15	CXOU J032615.2-212001	9.3	$5.6_{-0.9}^{+2.7}$	5.6 ± 1.5	0.50	yes	
16	CXOU J032622.6-212418	8.5	$5.5_{-1.2}^{+2.0}$	4.7 ± 1.4	4.3	no	
17	CXOU J032615.2-211924	2.9	$4.9_{-1.6}^{+2.1}$	1.5 ± 0.8	0.87	yes	A
18	CXOU J032617.1-212011	2.8	$4.5_{-1.6}^{+2.1}$	1.9 ± 2.2	0.082	yes	G
19	CXOU J032617.6-212013	2.8	$4.5_{-1.6}^{+2.0}$	2.0 ± 2.4	0.13	yes	G
20	CXOU J032622.8-211917	7.3	$4.4_{-0.9}^{+1.8}$	3.7 ± 1.1	1.5	no	
21	CXOU J032603.1-211921	7.4	$4.3_{-0.7}^{+2.3}$	3.7 ± 1.1	3.4	no	A, B
22	CXOU J032631.3-212339	5.8	3.9 ± 1.8	3.2 ± 1.2	4.8	no	
23	CXOU J032620.0-212023	5.7	3.4 ± 1.3	3.0 ± 1.1	0.69	yes	NG
24	CXOU J032616.3-211958	4.7	3.4 ± 1.8	2.7 ± 1.4	0.27	yes	G
25	CXOU J032622.4-212132	7.1	$3.2_{-0.8}^{+1.6}$	3.5 ± 1.1	1.8	no	NG
26	CXOU J032613.1-212020	4.7	$3.0_{-0.8}^{+1.3}$	2.3 ± 0.9	0.99	yes	NG
27	CXOU J032618.7-211814	5.9	$3.0_{-0.7}^{+1.5}$	3.1 ± 1.1	1.9	no	V
28	CXOU J032605.7-212058	5.3	$2.7_{-0.9}^{+1.1}$	2.6 ± 1.00	2.8	no	
29	CXOU J032619.0-212030	4.3	2.4 ± 0.9	2.2 ± 0.9	0.54	yes	G
30	CXOU J032619.4-212021	3.8	2.4 ± 1.0	2.0 ± 1.0	0.53	yes	G
31	CXOU J032619.3-212052	3.6	$2.3_{-1.1}^{+0.7}$	1.8 ± 0.8	0.88	yes	NG
32	CXOU J032619.9-212019	3.0	$2.3_{-0.9}^{+1.1}$	1.9 ± 1.00	0.64	yes	NG
33	CXOU J032616.4-211953	4.4	$2.3_{-0.7}^{+1.2}$	2.2 ± 1.0	0.31	yes	G
34	CXOU J032601.6-212021	3.6	$2.3_{-0.8}^{+1.1}$	1.8 ± 0.9	3.6	no	
35	CXOU J032625.5-211622	2.1	$2.3_{-0.9}^{+1.5}$	1.8 ± 1.1	4.2	no	C
36	CXOU J032618.3-212011	3.9	$2.3_{-0.9}^{+1.5}$	2.4 ± 1.2	0.25	yes	NG
37	CXOU J032621.6-211930	3.5	$2.2_{-0.9}^{+0.8}$	1.7 ± 0.8	1.2	no	NG
38	CXOU J032627.4-212235	5.7	$2.2_{-0.8}^{+1.4}$	2.9 ± 1.2	3.4	no	
39	CXOU J032616.2-211953	4.3	$2.1_{-0.7}^{+1.2}$	2.2 ± 1.0	0.34	yes	
40	CXOU J032615.5-211941	4.8	$2.1_{-0.7}^{+1.1}$	2.4 ± 1.0	0.60	yes	
41	CXOU J032602.2-212140	3.7	$2.0_{-0.9}^{+1.3}$	2.0 ± 1.2	3.8	no	
42	CXOU J032620.6-211713	3.6	$1.9_{-0.5}^{+1.3}$	1.8 ± 0.8	3.0	no	
43	CXOU J032613.9-211944	3.6	$1.8_{-0.5}^{+1.4}$	1.8 ± 0.8	0.87	yes	
44	CXOU J032610.3-211842	3.1	$1.8_{-0.7}^{+0.9}$	1.6 ± 0.8	2.1	no	
45	CXOU J032620.1-211958	2.3	$1.7_{-0.7}^{+0.9}$	1.2 ± 0.7	0.67	yes	NG
46	CXOU J032620.4-212112	3.0	$1.6_{-0.7}^{+0.9}$	1.5 ± 0.8	1.3	yes	NG
47	CXOU J032631.3-212210	3.2	$1.6_{-0.7}^{+1.1}$	1.6 ± 0.9	3.8	no	
48	CXOU J032624.2-212040	2.0	$1.6_{-0.9}^{+0.7}$	1.2 ± 0.8	1.7	yes	
49	CXOU J032620.6-212317	2.2	$1.5_{-0.7}^{+1.0}$	1.2 ± 0.8	3.2	no	
50	CXOU J032630.9-211824	3.3	$1.5_{-0.6}^{+0.9}$	1.7 ± 0.8	3.6	no	
51	CXOU J032606.7-212139	3.0	$1.4_{-0.5}^{+1.2}$	1.5 ± 0.8	2.9	no	V
52	CXOU J032621.9-212023	3.3	$1.3_{-0.5}^{+1.3}$	2.1 ± 1.00	1.1	yes	NG
53	CXOU J032614.6-211955	1.7	$1.3_{-0.5}^{+1.0}$	0.93 ± 0.70	0.65	yes	

TABLE 1
 SOURCES DETECTED (CONTD.)

Src	Name	Rate (10^{-4} s^{-1})	L_X^{spec} ($10^{38} \text{ erg s}^{-1}$)	L_X^{rate} ($10^{38} \text{ erg s}^{-1}$)	ΔR ($''$)	In D_{25}	Comment
54	CXOU J032620.5-212041	2.5	$1.3^{+0.7}_{-0.6}$	1.3 ± 0.7	0.94	yes	G
55	CXOU J032613.9-212005	2.1	$1.2^{+1.1}_{-0.4}$	1.1 ± 0.7	0.79	yes	
56	CXOU J032625.1-212043	2.0	$1.1^{+1.0}_{-0.4}$	1.1 ± 0.7	1.9	yes	
57	CXOU J032621.8-211930	2.6	$1.1^{+0.5}_{-0.7}$	1.3 ± 0.7	1.2	no	NG
58	CXOU J032609.2-212156	1.5	$1.1^{+0.5}_{-0.7}$	0.81 ± 0.66	2.6	no	
59	CXOU J032622.8-211620	1.4	$1.1^{+0.8}_{-0.5}$	0.76 ± 0.64	4.0	no	
60	CXOU J032623.1-211945	1.6	$1.1^{+0.7}_{-0.5}$	0.79 ± 0.60	1.4	no	NG
61	CXOU J032616.5-211920	1.7	1.0 ± 0.6	0.83 ± 0.63	0.81	yes	
62	CXOU J032634.7-211755	2.0	$0.96^{+1.2}_{-0.36}$	1.1 ± 0.7	4.6	no	
63	CXOU J032615.4-211948	2.1	$0.96^{+1.1}_{-0.34}$	1.0 ± 0.7	0.53	yes	
64	CXOU J032612.8-211960	2.1	$0.93^{+1.1}_{-0.33}$	1.1 ± 0.7	1.0	yes	
65	CXOU J032615.7-212038	2.6	0.93 ± 0.57	1.3 ± 0.8	0.63	yes	NG
66	CXOU J032620.8-211957	1.4	$0.88^{+0.84}_{-0.40}$	0.73 ± 0.61	0.83	yes	G
67	CXOU J032621.5-212029	1.3	$0.82^{+0.63}_{-0.49}$	0.68 ± 0.62	1.1	yes	G
68	CXOU J032616.6-211927	1.6	$0.79^{+0.97}_{-0.31}$	0.79 ± 0.65	0.69	yes	
69	CXOU J032604.7-211613	1.7	$0.78^{+0.60}_{-0.46}$	0.89 ± 0.66	4.8	no	
70	CXOU J032607.9-211828	1.5	$0.75^{+0.63}_{-0.43}$	0.77 ± 0.61	2.7	no	
71	CXOU J032618.8-212148	1.4	$0.63^{+0.56}_{-0.37}$	0.69 ± 0.60	1.7	no	R(?), NG
72	CXOU J032614.2-211950	1.4	$0.63^{+0.57}_{-0.45}$	0.75 ± 0.67	0.76	yes	
73	CXOU J032615.7-212017	1.2	$0.34^{+0.55}_{-0.28}$	0.61 ± 0.59	0.39	yes	NG

NOTE. — Source list for all point-sources detected on the *ACIS* S3 chip, excluding the source coincident with NGC 1331. Two luminosity estimates are given, L_X^{spec} and L_X^{rate} which are, respectively, the luminosity estimated from the spectra and from the count-rate (exposure-corrected). ΔR is the distance of the source from the galaxy centroid (in arcmin). The count-rate column quotes count-rates *not* corrected for exposure-map variations. The comment abbreviations are as follows: A—absorbed spectrum, B—soft spectrum, C—close to chip edge (flux may be a unreliable), E—extended, G—coincident with a globular cluster, NG—in the WFPC2 fov but not coincident with a GC, R—also seen with *Rosat* and V—variable.

 TABLE 2
 COMPOSITE SOURCE SPECTRA

Model	χ^2/dof	N_H 10^{22} cm^{-2}	Γ	kT (keV)
All sources				
power law	122/119	0.0223	1.40 ± 0.05	
	115.3/118	0.07 ± 0.03	1.5 ± 0.1	
bremsstrahlung	115/119	0.0223		15^{+6}_{-4}
	114/118	0.03 ± 0.02		12^{+7}_{-3}
Sources in D_{25} only				
power law	50.0/46	0.0223	1.55 ± 0.10	
	50.0/45	< 0.075	1.6 ± 0.1	
bremsstrahlung	50.8/46	0.0223		8^{+4}_{-2}
	49.2/45	< 0.031		10^{+5}_{-3}

NOTE. — Results of fitting the composite spectra of all the point sources on the *ACIS*-S3 chip and, separately, only those sources in the D_{25} region. N_H values shown include the Galactic column density, which was $0.0223 \times 10^{22} \text{ cm}^{-2}$ (Dickey & Lockman 1990). Where no error-bars are shown the parameter was fixed. Errors are 90% confidence intervals.